

INVERSION OF ELECTRICAL CAPACITANCE TOMOGRAPHY DATA BY SIMULATED ANNEALING: NON-LINEAR VERSUS LINEARIZED FORWARD MODELING

R. Martin¹, C. Ortiz-Aleman¹, J. C. Gamio¹, and S. Muñoz-Gonzalez¹

¹*Instituto Mexicano del Petroleo, Mexico*
Email: jcortiz@imp.mx

Received 31 January 2005; accepted 19 August 2005

ABSTRACT

In this work we apply the simulated annealing (SA) inversion method to the reconstruction of permittivity images from electrical capacitance tomography (ECT) data. We test the SA inversion method using static physical models simulating some typical distribution patterns of two and three-component flows. The SA-based permittivity inversions have some advantages over other approaches based on linear least-squares inversion: they can find good solutions starting with poor initial models, can more easily implement complex a priori information, and do not introduce smoothing effects in the final permittivity distribution model. A major disadvantage comes from the fact that SA is computationally intensive and lead to relatively slow reconstructions. We establish comparisons between two variations of the SA inversion method: a first one where computation of the forward problem (i.e., to find the mutual capacitance data for a given permittivity distribution inside the sensor) is made in a non-linear fashion by using a finite-volume method (FVM); and a second one, where we employed a linearized numerically improved forward model based on the use of a sensitivity matrix. We found this last approach to be faster and more accurate than traditional linear methods. Finally, results of this work provided us some insight about the effects on permittivity estimation from ECT data caused by linearization of the forward model.

Keywords: Capacitance tomography, simulated annealing, image reconstruction, finite volume method, sensitivity matrix.

1 INTRODUCTION

Tomography methods are mainly employed for obtaining estimated images of a cross section of an object. X-ray tomography was the first to be developed (in 1960s) and its use is now routine not only in medicine but in some industrial applications as well (internal inspection of mechanical components and flaw detection in materials, for example). Since then a number of new tomography methods aimed at industrial processes have emerged, collectively known as process tomography (Williams and Beck 1995).

The main goal of process tomography methods, which started to develop in the mid 1980s, is to produce an image of the phase or component distribution in an industrial process using only external sensors and without causing any perturbation to it (Figure 1).

In other words, process tomography provides a way of 'looking' inside the process, from the outside and with no need for physical intrusion or alteration, in a radically new global approach to gathering structural information on the process, unlike the traditional methods based on local sampling. Examples of suitable processes are those occurring in mixing or stirring vessels, fluidized bed reactors, separator tanks, or a pipeline carrying multiphase flow.

There is a whole range of principles and techniques that can be exploited in process tomography, including electrical methods based on impedance measurement, ultrasound, magnetic resonance, optical methods and those based on ionizing radiation (X- and gamma-rays). Generally speaking, ionizing radiation methods produce images with the highest definition, but are relatively slow to achieve. On the other hand, electrical methods yield low-resolution images but are much faster, robust and relatively inexpensive. In particular with regard to electrical impedance tomography, or electrical tomography for short, there has been a very noticeable progress in the last few years. This type of tomography has two main modalities: capacitance and resistance tomography. In electrical capacitance tomography or ECT (Beck *et al.* 1997; Gamio 1997; Plaskowski *et al.* 1995), normally used with mixtures where the continuous phase is non-conducting, the sensor employed (Figures 1 and 2) is made of a circular array of electrodes distributed around the cross-section to be examined, and the capacitance between all the different electrode-pair combinations is measured. With the help of a computer and a suitable image reconstruction algorithm, this information is used to create a map showing the variation of the dielectric constant (or relative permittivity) inside the sensor area, thus providing an indication of the physical distribution of the various components of the mixture. In this particular case, the electrodes can be located on the outside of a non-conducting pipe, in order to simplify sensor construction and avoid direct contact with the process fluids. A second external grounded metallic pipe serves as an electric screen and to provide mechanical resistance.

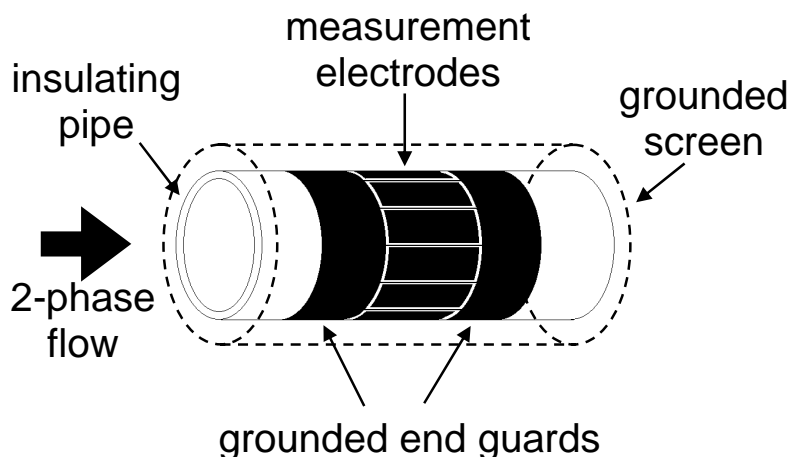


Figure 1: Capacitance tomography sensor.

In principle, ECT has important applications in multiphase flow measurement, particularly gas-oil two-phase flow, which often occurs in many oil wells. The traditional way to quantify the various fluids produced by an oil well is to separate the mixture by gravity in large tanks, prior to measuring each component separately using conventional single-phase flow meters.

where c_{ii} are the self-capacitance coefficients (or just self-capacitance for short) of electrode i , while the others, c_{ij} , with $i \neq j$, are the mutual capacitance coefficients (or just mutual capacitance) between electrodes i and j . Put in matrix form, equation (1) becomes

$$\begin{bmatrix} q_1 \\ q_2 \\ \vdots \\ q_n \end{bmatrix} = \begin{bmatrix} c_{11} & c_{12} & \cdots & c_{1n} \\ c_{21} & c_{22} & \cdots & c_{2n} \\ \vdots & \vdots & \ddots & \vdots \\ c_{n1} & c_{n2} & \cdots & c_{nn} \end{bmatrix} \begin{bmatrix} v_1 \\ v_2 \\ \vdots \\ v_n \end{bmatrix} \quad (2)$$

or

$$\mathbf{q} = \mathbf{C} \mathbf{v} \quad (3)$$

Since the capacitance have the property of reciprocity, i.e., $c_{ij} = c_{ji}$, there are only $m = \frac{1}{2}n(n-1)$ independent mutual capacitance, corresponding to lower (or upper) triangular matrix of \mathbf{C} , and corresponding also to each one of the m different electrode- pairs that can be formed in the sensor.

The value of the mutual capacitance is a complex non-linear function of the conductor system geometry, and of the spatial distribution of the dielectric constant or relative permittivity of the dielectric medium. In the case of the ECT sensor, the geometry of the electrodes, that of the pipe, and the value of the dielectric constant of the latter, are all fixed. Therefore, it can be said that the mutual capacitance are a function only of the spatial distribution of the dielectric constant inside the sensor, $\varepsilon(x,y)$. The problem of calculating the mutual capacitance corresponding to a specific permittivity distribution inside the sensor is referred to as the forward problem.

The use of the cylindrical end guards (Figure 2) and the assumption that the phase (and thus the permittivity) distribution does not change too much in the axial direction, allows the sensor to be represented by a two-dimensional (2-D) model (Xie *et al.* 1989). Unless otherwise stated explicitly, in what follows a 2-D model of the sensor will be used. Therefore, the electric charges q_i and the capacitance c_{ii} and c_{ij} that appear in equations (1) and (2) should be considered quantities per unit length of the electrodes in the axial direction. A tilde (i.e., \tilde{q}_i , \tilde{c}_{ii} and \tilde{c}_{ij}) shall be used to denote the total quantities that result from considering the actual length of the electrodes. The previous variables are related between them through the electrode length L , according to

$$q_i = \frac{\tilde{q}_i}{L} \quad , \quad c_{ii} = \frac{\tilde{c}_{ii}}{L} \quad \text{and} \quad c_{ij} = \frac{\tilde{c}_{ij}}{L} \quad (4)$$

If the interior of the 2-D sensor is divided into p equal-area regions (or 'pixels') where the permittivity is considered constant, then the discrete version of the forward problem is

$$\mathbf{c} = \begin{bmatrix} c_1 \\ \vdots \\ c_m \end{bmatrix} = \mathbf{f}(\boldsymbol{\varepsilon}) = \begin{bmatrix} f_1(\boldsymbol{\varepsilon}) \\ \vdots \\ f_m(\boldsymbol{\varepsilon}) \end{bmatrix} \quad \text{with} \quad \boldsymbol{\varepsilon} = \begin{bmatrix} \varepsilon_1 \\ \vdots \\ \varepsilon_p \end{bmatrix} \quad (5)$$

where \mathbf{c} is the vector of mutual capacitance (per unit length), f_i are non-linear functions not known explicitly and $\boldsymbol{\varepsilon}$ is the vector of permittivity corresponding to the p regions or pixels within the sensing zone.

Applying Gauss's Law, the mutual capacitance per unit axial electrode length can be calculated as

$$c_{ij} = \frac{q_i}{v_j} = -\frac{\varepsilon_o}{V} \oint_{\Gamma_i} (\boldsymbol{\varepsilon} \nabla \phi^j) \cdot d\mathbf{l} = -\frac{\varepsilon_o}{V} \oint_{\Gamma_i} \boldsymbol{\varepsilon} \frac{\partial \phi^j}{\partial n} dl \quad (6)$$

where ε_o is the permittivity of free space, equal to 8.854×10^{-12} farads per meter, Γ_i is a closed curve surrounding electrode i , $d\mathbf{l}$ is a normal vector representing an element of the curve Γ_i , dl is an element of length of that curve, the symbol ' \cdot ' represents the scalar product of two vectors, and ϕ^j is the electrostatic potential produced in the sensor when applying a voltage of V volts to electrode j (which is called source or excitation electrode) and 0 volts to all others (called detection electrodes).

The potential ϕ^j is determined by the solution of the following partial differential equation

$$\nabla \cdot \boldsymbol{\varepsilon}(x, y) \nabla \phi^j = 0 \quad (7)$$

subject to the boundary conditions (a) $\phi^j = V$ volts on the source electrode and (b) $\phi^j = 0$ on the detection electrodes and the outer screen. In general, equation (7) does not have an analytic solution and must be solved numerically.

The problem of estimating what is the spatial permittivity distribution inside the sensor that corresponds to a specific set of mutual capacitance values is referred to as the inverse problem, and is the problem that image reconstruction methods must address and solve. Normally, the permittivity estimation is made in a discrete way, representing it as a vector $\boldsymbol{\varepsilon}$ like the one in equation (5), which must be calculated from a vector of observed mutual capacitance \mathbf{c} , obtained using a suitable measurement apparatus.

Most of the currently used ECT image reconstruction methods are linear and they have the problem that they require, for their correct operation, one or more regularization parameters whose right value is strongly dependent, precisely, on the image that one wishes to reconstruct, implying that one would need to know beforehand the solution to the problem. Moreover, these methods generally produce distorted images, because the regularization has an excessive smoothing effect on the obtained permittivity. If the regularization is too strong the smoothing effect will occur, and if it is too weak the method can become unstable and/or not converge to the desired solution. Most of these problems are related to the fact that local optimization algorithms, during their search, explore only a relatively small sector of the solution domain, restricted to the vicinity of the initial guess. If the optimal solution of the problem, i.e., the absolute minimum of the objective function, is located far from the initial guess, it will hardly be reached due to the presence of relative minima in their way, places where these methods can become trapped. The most used methods in this category are least-squares linear inversion and techniques that utilize the gradient of the objective function, like the steepest-descent and the conjugate-gradient methods.

In general, local search methods exploit the scarce information derived from the comparison of a small number of models, thus avoiding an extensive search in the whole model space (Sambridge and Drijkoningen 1992).

On the other hand, global optimization methods, as SA, explore the whole solution domain during the inversion process. They carry out an extensive scan within the model space. In this way, despite the existence of partial solutions to the problem, there is a greater possibility that the final solution corresponds to the best fit between the observed and the synthetic data. This type of methods, contrary to local techniques, does not require the information provided by the derivatives of the objective function, because in this case the problem does not need to be linearized. Global optimization algorithms use stochastic criteria in order to simultaneously explore all the solution space in search of the optimal model. The best known of the global methods is Monte Carlo, which performs a purely random and unbiased search. In other words, when generating each new model, it does not take advantage of the information obtained from the previously evaluated models (Gallagher *et al.* 1991). The unguided randomness is the most characteristic feature of this method, which distinguishes it from the rest of the global methods. Among the global optimization techniques, there are also the methods of SA and genetic algorithms (GA). Both were conceived as analogies of optimization systems occurring in nature. GA emulates the mechanisms of biological evolution while SA is based on thermodynamics. Both methods are inherently non-linear and, therefore, lend themselves naturally to their application in capacitance tomography, a non-linear problem.

2 INVERSION BY SIMULATED ANNEALING (SA)

The SA method is based on an analogy with the thermodynamic process of crystallisation. A mineral fluid that cools slowly until it reaches a low energy state, gives rise to the formation of well defined crystals. If, on the contrary, the substance leaves its thermal equilibrium state with a sudden or partial cooling, the resulting crystal will have many defects, or the substance may even form a 'glass', characterised by its meta-stable molecular disorder. This concept is used in the context of optimisation methods to recognise potentially useful models or configurations.

The atoms of each molecular configuration are equivalent to the model parameters in the inverse problem (i.e., the permittivity of the various image pixels). The system energy for such configuration is related to the energy function associated with the set of parameters involved in the model. A least squares solution can be achieved by minimising this energy function E which is defined as the difference between the observed ($c_{k\text{ obs}}$) and synthetic ($c_{k\text{ calc}}$) data:

$$E = \frac{\sum_{k=1}^m ((c_{k\text{ obs}}) - (c_{k\text{ calc}}))^2}{\sum_{k=1}^m (c_{k\text{ obs}})^2} \quad (8)$$

where m is the number of inter-electrode capacitance measurements.

The method of SA has three basic components (Ingber 1989): an energy (or cost, or misfit) function, an order function (the Metropolis criterion), and a set of parameters that control the temperature for each model parameter. The process consists of three nested cycles (Figure 3). The external cycle (3) regulates the system temperature. Every time a cycle is completed, the temperature for each parameter decreases as its initial temperature is multiplied by a factor. In this way the desired slow and gradual cooling is carried out. The intermediate cycle (2) generates a set of constants K_i associated to each parameter. Said constants determine the change that each parameter may experience. In the inner cycle (1), the parameter values are perturbed by multiplying each parameter by the product of its corresponding K_i times a randomly chosen number between minus one and one.

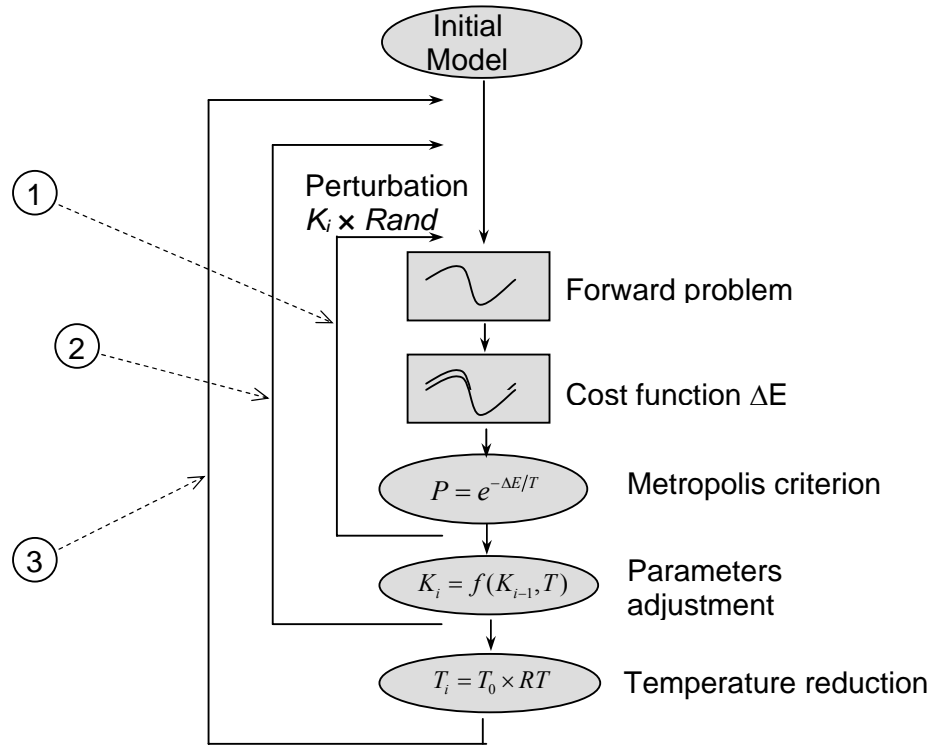


Figure 3: Implementation of the SA method (after Ortiz-Aleman *et al.* 2004).

The synthetic response of the current model is calculated and the change in the system's energy associated to the new parameter configuration is evaluated. This shift causes a change ΔE in the system's total energy. If ΔE is less than or equal to zero, the change in the parameter is accepted and the resulting configuration is considered as the new current configuration. When there is an increase in the system energy (ΔE is greater than zero), the probability of acceptance or rejection for the parameter change is determined, according to the Metropolis criterion (Metropolis *et al.* 1953), as

$$P(\Delta E) = e^{-\Delta E/T} \quad (9)$$

In order to decide whether or not a change that produces an increase in the system energy is accepted a random number between zero and one is generated, which is then compared with the value of the probability corresponding to ΔE .

If said random number is greater, the parameter shift is not accepted and the configuration that existed before the shift is maintained. Repeating this procedure continuously, the thermal movement of the atoms of a system in thermal equilibrium (at a fixed temperature T) is simulated. In order to reach the system's base state, that is to say, the state of lowest energy and highest order, the temperature for each parameter must be reduced very slowly, simulating a quasi-static process. This means that, during the cooling, the system must experience a series of states infinitesimally separated from the state of thermal equilibrium.

The three cycles are repeated, while the temperature of the process decreases progressively. As the temperature diminishes, the parameter variations are smaller and smaller. In this way, the search in the solutions domain tends to confine itself towards the models associated with the global minimum of the energy function.

3 NONLINEAR FORWARD PROBLEM SOLUTION BY THE FINITE VOLUME METHOD (FVM)

The forward problem consists in calculating the mutual capacitance c_{ij} , $i \neq j$, that result from the presence of a permittivity distribution ϵ inside the sensor. As we mentioned in the previous section, the SA method requires the repeated solution of the forward problem. Because of that, it is very important to have a suitable method to solve said problem, that achieves a reasonable balance between accuracy (or precision) and speed.

In this section, the forward problem, described by equation (7), is solved using the finite-volume method in a cylindrical configuration. In this way, the undetermined solutions in the center of the disc (which is a problem for other methods like the finite-difference method) are eliminated and the mesh refinement becomes more flexible as compared to finite-element methods. The equation is subject to the boundary conditions (a) $\phi^k = V$ volts on the source electrode and (b) $\phi^k = 0$ on the detection electrodes and on the outer screen.

Defining the radial and angular coordinates as r and θ , and using the finite-volume method, the discrete equation is formulated in conservative form for each cell Ω_{ij} as

$$\int_{\Omega_{ij}} \nabla \cdot (\epsilon \nabla \phi^k) d\Omega_{ij} = 0 \quad \text{for} \quad i = 1, \dots, N_r \quad \text{and} \quad j = 1, \dots, N_\theta \quad (10)$$

where i and j refer to the discretization in r and θ , respectively, and N_r and N_θ are the number of sections into which the radius and the circumference are divided, respectively.

Applying Gauss's theorem in polar coordinates, the discrete equations can be written as

$$\int_{\Gamma_{ij}} \epsilon \nabla \phi^k \cdot d\Gamma_{ij} = 0 \quad (11)$$

where Γ_{ij} is the boundary of the finite volume cell Ω_{ij} . The boundary Γ_{ij} is defined by Γ_W and Γ_E along the radial coordinates, and by Γ_N and Γ_S along the angular coordinates. Equation (11) can be expressed as the sum of the fluxes through the faces Γ_N , Γ_S , Γ_E and Γ_W

$$\begin{aligned} \sum_l \left(\int_{\Gamma_l} \varepsilon \nabla \phi^k \cdot n_l \, d\Gamma_l \right) &= \left(\frac{\varepsilon}{r} \frac{\partial \phi^k}{\partial \theta} \Delta r \right) \Big|_{\left(i+\frac{1}{2}\right),j} - \left(\frac{\varepsilon}{r} \frac{\partial \phi^k}{\partial \theta} \Delta r \right) \Big|_{\left(i-\frac{1}{2}\right),j} \\ &+ \left(\varepsilon \frac{\partial \phi^k}{\partial \theta} r \Delta \theta \right) \Big|_{i,\left(j+\frac{1}{2}\right)} - \left(\varepsilon \frac{\partial \phi^k}{\partial \theta} r \Delta \theta \right) \Big|_{i,\left(j-\frac{1}{2}\right)} \end{aligned} \quad (12)$$

From equation (12), the term corresponding to the fluxes at zero radius vanishes and the problem is equivalent to solving the equations in the proximity of the center on triangles that have a vertex on the center. Then, the discrete system of equations for the forward problem is well posed. The complete system is similar to a Laplacian system of equations, and a diagonal banded system that includes the periodic boundary conditions imposed by the problem geometry must be solved. The corresponding matrix is positive definite and symmetric, characteristics that were exploited when selecting the conjugate gradient method for its solution.

Finally, the mutual capacitance was calculated by integrating the potential gradients along a curve surrounding the electrodes, according to equation (6). The integration is done using a trapezoidal rule and the potential gradients were calculated to the fourth order.

During the procedure for reconstructing a permittivity image using SA, it is necessary to solve the forward problem and find the electric potential repeatedly for relatively similar successive permittivity distributions, while the method converges towards the final solution. Since the potential corresponding to said successive distributions changes relatively little, it is possible to accelerate the whole process if an iterative method is used to solve the forward problem, taking as the first guess for the current potential the solution corresponding to the previous permittivity configuration. Because the initial guess for the potential will be quite close to the solution, said iterative method will converge in less iterations, rapidly achieving an acceptable accuracy.

4 LINEARIZED FORWARD PROBLEM SOLUTION

In order to get a fast linearized version of the forward problem, we made use of a recently introduced procedure (Ortiz-Aleman and Martin 2005). Following that approach, a sensitivity matrix is computed as

$$S_{ik} = \frac{C_i^k - C_{i(emp)}}{C_{i(full)} - C_{i(emp)}} \quad \text{for } i = 1, \dots, m \quad \text{and } k = 1, \dots, p \quad (13)$$

where k is the pixel number (from 1 to p), C_i^k is the capacitance measured with electrode pair i when the area of pixel k is full of a high-permittivity material while the rest of the sensor is full of a low-permittivity material, whereas $C_{i(full)}$ and $C_{i(emp)}$ are the capacitance for electrode pair i when the sensor is full of high- and low-permittivity material, respectively. These sensitivity maps were calculated by solving numerically equation (7) with the finite volume method (FVM) and applying equation (6). Having determined the sensitivity maps, they can

be used for obtaining ECT synthetic data, from any permittivity distribution inside the sensor. For this purpose, the measured capacitance data must be normalized according to:

$$\tilde{c}_i = \frac{C_i - C_{i(emp)}}{C_{i(full)} - C_{i(emp)}} \quad \text{for } i = 1, \dots, m \quad (14)$$

where \tilde{c}_i is the normalized capacitance for electrode pair i and C_i is the actual capacitance measured with that electrode pair.

In this way, the linear forward problem in ECT can be written in matrix form as:

$$\tilde{\mathbf{S}}\tilde{\boldsymbol{\varepsilon}} = \tilde{\mathbf{c}} \quad (15)$$

where $\tilde{\mathbf{c}}$ is a vector of normalized capacitance data, $\tilde{\boldsymbol{\varepsilon}}$ is a vector of normalized model permittivity, and $\tilde{\mathbf{S}}$ is the normalized sensitivity matrix. Normalization of model permittivity and the sensitivity matrix was performed by using the next expressions:

$$\tilde{\varepsilon}_i = \frac{\varepsilon_i - \varepsilon_{i(emp)}}{\varepsilon_{i(full)} - \varepsilon_{i(emp)}} \quad \text{for } i=1, \dots, p \quad (16)$$

$$\tilde{s}_{ik} = \frac{s_{ik}}{\sum_{k=1}^p s_{ik}} \quad \text{for } i = 1, \dots, m \quad \text{and } k = 1, \dots, p \quad (17)$$

During the process of reconstructing a permittivity image using SA, it is necessary to solve the forward problem repeatedly for quite similar successive permittivity distributions, while the method converges towards the global solution. Since the solution corresponding to said successive permittivity distributions changes relatively little, it is possible to accelerate the whole process by taking into account the solution corresponding to the previous permittivity configuration. Because this previous guess will be quite close to the next solution, the number of floating-point operations can be dramatically reduced by removing the entire redundant matrix by vector multiplications involved in the computation of the forward problem described by equation (15). To illustrate this numerical improvement of the method, let us consider the case when parameter ε_i is being perturbed:

$$\begin{bmatrix} \tilde{s}_{11} & \dots & \tilde{s}_{1i} & \dots & \tilde{s}_{1p} \\ \tilde{s}_{21} & \dots & \tilde{s}_{2i} & \dots & \tilde{s}_{2p} \\ \vdots & \dots & \dots & \ddots & \vdots \\ \tilde{s}_{m1} & \dots & \tilde{s}_{mi} & \dots & \tilde{s}_{mp} \end{bmatrix} \begin{bmatrix} \tilde{\varepsilon}_1 \\ \vdots \\ \tilde{\varepsilon}_i + \Delta\tilde{\varepsilon}_i \\ \vdots \\ \tilde{\varepsilon}_p \end{bmatrix} = \begin{bmatrix} \tilde{c}_1 \\ \vdots \\ \vdots \\ \tilde{c}_m \end{bmatrix} \quad (18)$$

where $\Delta\varepsilon_i$ is the change that parameter ε_i may experience in the inner cycle of the SA method. Therefore, computation of a new set of ECT synthetic data can be made by adding a correction factor to the previously computed ECT data vector. That is,

$$\begin{bmatrix} \tilde{c}_1^{new} \\ \vdots \\ \tilde{c}_m^{new} \end{bmatrix} = \begin{bmatrix} \tilde{c}_1^{old} \\ \vdots \\ \tilde{c}_m^{old} \end{bmatrix} + \Delta \tilde{\mathcal{E}}_i \begin{bmatrix} \tilde{s}_{1i} \\ \vdots \\ \tilde{s}_{mi} \end{bmatrix} \quad (19)$$

In this way, the inversion process is accelerated and CPU time consumption is comparable to other iterative linear inversion methods.

5 RESULTS

In a previous work (Ortiz-Aleman *et al.* 2004), we followed the advice of (Yang and Peng 2003) to test non-linear methods for both forward modelling (using the finite volume method) and reconstruction of electrical permittivity images by means of global inversion methods (SA). In this paper we apply again the SA method in order to establish comparisons between two different SA-based inversion approaches: the one describes in section 3, based on non-linear forward modelling by using finite volumes; and a linear approximation by means of a numerically improved sensitivity matrix approach, introduced in section 4. When using this last approach, we employed a sensitivity matrix computed for a set of 1333 elements or pixels. In the case of the non-linear approach, we used a 240×120 grid size for the forward problem computations by the finite volume method.

In a first set of tests, we applied both variations of the SA method to ECT synthetic data computed for three permittivity distributions (see Figure 4). We simulated a twelve-electrode ECT sensor and we computed the capacitance values for all single-electrode combinations. For the first study case (Figure 4A), we modeled a three-component distribution with permittivity values of air (1.0), an intermediate permittivity material (1.8), and oil (2.5). In the second (Figure 4B) and third test cases (Figure 4C), we considered two-component distributions simulating idealized patterns for bubbly flows, with a lower permittivity material of 1.0 (air) and a higher permittivity material of 2.5 (oil). In all these cases, we added a random noise level of 3% on the synthetic ECT data.

In Figure 4 we show the ideal permittivity images to be inverted on the left column and their corresponding reconstructed images when using linear (in the middle) and non-linear (on the right column) forward modelling. In figure (4A), we can notice one of the effects of the normalisation applied on both the sensitivity matrix and capacitance data as a part of the process of linearization: when using linear forward modelling, as the iterative process goes on, permittivity estimation tend to values in the close neighbourhood of the top and bottom limits of the chosen normalised range. As a consequence of this trend, objects appear somewhat distorted respect to their real shape and relative size. In the other two cases (Figures 4B and 4C) results are similar for both approaches but objects are better defined on the non-linear case. We stopped the process of inversion of permittivity images at 100,000 computations of the forward problem in all cases. In terms of computing time, the linear approximation resulted ~ 100 times faster than the non-linear approach.

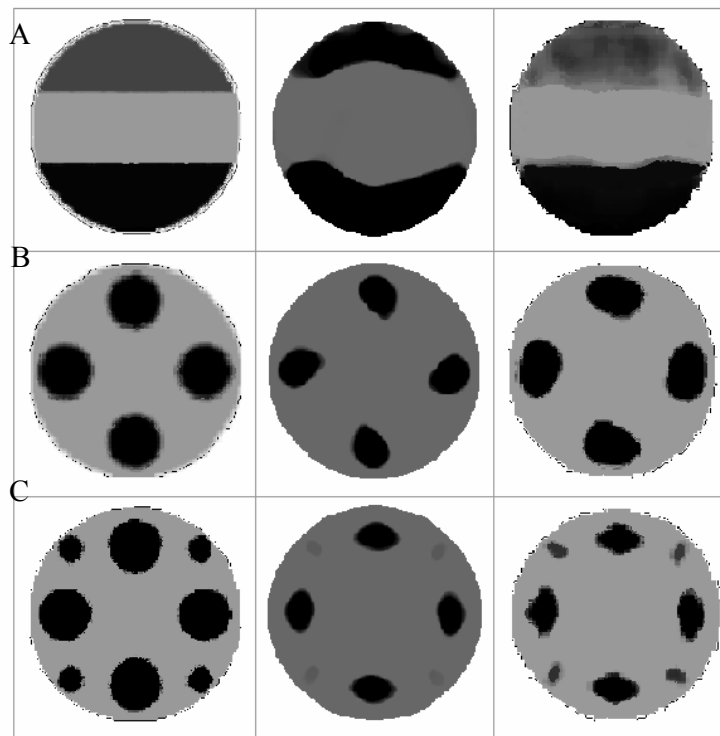


Figure 4: Image reconstruction of synthetic ECT data. Ideal distributions are depicted on the left column, reconstructions by non-linear forward problem computation are in the middle, and linear forward modelling results are on the right. Test cases correspond to: (A) simulation of a stratified flow of three-components; (B) flow with four large size bubbles; (C) flow with four large bubbles and four small size bubbles. Reconstructed images were achieved after 100,000 iterations of the SA method. Black and white represent top and low permittivity values, respectively (see text).

For comparisons between image reconstruction of synthetic ECT data by the SA method and by other commonly used linear approaches, the reader is referred to (Ortiz-Aleman *et al* 2004). In this work we also focused our attention on the inversion of measured ECT data, which always imply a higher degree of complexity relative to the inversion of synthetic data.

In a first case (Figure 5A), we placed a perspex rod on the left side of the sensor and a nylon rod on the right. For both kind of approaches, we got reconstructed images with two slightly distorted circular objects located on the right positions and with roughly the same size as the simulated rods. Elongation of the nylon rod and distortion to the right of the perspex rod are related to the kind of mesh that we employed for the computation of the estimated permittivity distribution. In the case of the linear approach, another cause for such distortion on the shape is associated to the process of normalisation of the sensitivity and capacitance data. As mentioned above, this normalisation process tends to guide the search for the optimum model to the close vicinity of the upper and lower bounds of each parameter value. As in the case of synthetic data, reconstruction of three different components (two rods with different permittivity values, and air) leads to a distortion on the shape of the object with intermediate permittivity value (the nylon rod located on the right side).

A second case consisted in locating a plastic bottle with air in the middle of the sensor completely full of polypropylene beads (see Figure 5B). The reconstructed images resultant from both approaches reproduce the shape and location of the bottle. In the case of the linear forward model some phantoms of low permittivity value can be seen close to the sensor wall and surrounding the bottle maybe due to the presence of a significant amount of air filling gaps. On the other hand, the non-linear approach was able to locate a great deal of small-size high-permittivity features clearly associated to the presence of the polypropylene beads.

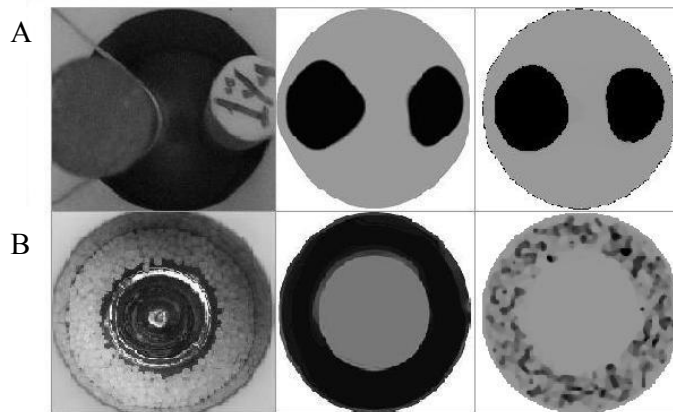


Figure 5: Image reconstruction of measured ECT data. Test distributions are depicted on the left column, reconstructions by non-linear forward problem computation are in the middle, and linear forward modelling results are on the right. Test cases correspond to: (A) Perspex rod on the left side of the sensor and nylon rod on the right; (B) plastic bottle with air in the middle of the sensor completely full of polypropylene beads. Reconstructed images were achieved after 100,000 iterations of the SA method. Black and white represent top and low permittivity values, respectively (see text).

6 CONCLUSIONS

Applying SA to the inversion of synthetic and measured data has provided us promising results. Application of linear forward modelling and SA for the inversion of measured ECT data made possible to overcome the major disadvantage of the SA method relative to linear methods: its much higher computation time. As SA requires several thousands of iterations (instead of a few hundreds for linear methods), numerical improvements on the forward problem computation were required in order to significantly reduce its numerical burden. In the case of two-component simulations, we observed a similar performance as in the case of the application of global SA optimisation and FVM forward modelling.

A main disadvantage of the linear approach, relative to the non-linear case, comes from the fact that it causes a major degree of distortion on the shape of the objects which is associated to the process of normalisation of the sensitivity and capacitance data. This normalisation process tends to guide the search for the optimum model to the close vicinity of the upper and lower bounds of each parameter value. Thus, when dealing with three different components such distortion on the shape is especially enhanced for the object with the intermediate permittivity value.

The SA method produced satisfactory image reconstructions for all the studied cases. As a consequence, we found the SA method as a fast and efficient technique for routine interpretation of measured ECT data, and also as a valuable post-processing tool for high quality imaging.

7 ACKNOWLEDGEMENTS

We thank W.Q. Yang for his kind support on implementation of inversion algorithms applied to electrical capacitance tomography. M. Sen helped the authors with valuable advice on the use of the simulated annealing algorithm. This contribution was supported by projects IMP/D.00117, IMP/D.00046 and IMP/D.00320.

REFERENCES

Beck MS, Byars M, Dyakowski T, Waterfall R, He R, Wang SM, and Yang WQ (1997). Principles and industrial applications of electrical capacitance tomography. *Measurement + Control* Vol. 30, pp. 197-200.

Gallagher K, Sambridge M, and Drijkoningen G (1991). Genetic algorithms: an evolution from Monte Carlo Methods for strongly non-linear geophysical optimization problems. *Geophys. Res. Lett.* 18, pp. 2177-2180.

Gamio JC (1997). A High-sensitivity Flexible-excitation Electrical Capacitance Tomography System. *PhD Thesis, University of Manchester Institute of Science and Technology, UK.*

Hammer EA and Johansen GA (1997). Process tomography in the oil industry: state of the art and future possibilities. *Measurement + Control* Vol. 30, pp. 212-216.

Ingber, L (1989). Very fast simulated re-annealing. *Journal of Mathematical and Computer Modelling* 12, pp. 967-973.

Metropolis N, Rosenbluth A, Rosenbluth M, Teller A, and Teller E (1953). Equation of state calculations by fast computing machines. *J. Chem. Phys.* 21, pp. 1087-1092.

Ortiz-Aleman C, Martin R, and Gamio JC (2004). Reconstruction of permittivity images from capacitance tomography data by using very fast simulated annealing. *Measurement Science and Technology* 15, pp. 1382-1390

Ortiz-Aleman C and Martin R (2005). Inversion of electrical capacitance tomography data by simulated annealing: Application to real two-phase gas-oil flow imaging. *Flow Measurement and Instrumentation* 16, pp. 157-162.

Plaskowski A, Beck MS, Thorn R, and Dyakowski T (1995). *Imaging Industrial Flows: Applications of Electrical Process Tomography.* Institute of Physics Publishing, UK.

Sambridge M and Drijkoningen G (1992). Genetic algorithms in seismic waveform inversion. *Geophys J. Int.* 109, pp. 323-342.

Thorn R, Johansen GA, and Hammer EA (1997). Recent developments in three phase flow measurement. *Measurement Science and Technology* 8, pp. 691-701.

Williams RA and Beck MS (eds) (1995). *Process Tomography - Principles, Techniques and Applications*. Butterworth Heinemann.

Xie CG, Plaskowski A and Beck MS (1989). 8-electrode capacitance system for two-component flow identification. Part 1: Tomographic flow imaging. *IEE Proceedings A* 136 (4), pp. 173-183.

Yang WQ and Peng L (2003). Image reconstruction algorithms for electrical capacitance tomography. *Measurement Science and Technology* 14(1), pp. R1-R13.